EF-G-Dependent GTPase on the Ribosome. Conformational Change and Fusidic Acid Inhibition †

ARTICLE *in* BIOCHEMISTRY · MARCH 2006

Impact Factor: 3.02 · DOI: 10.1021/bi0516677 · Source: PubMed

6 AUTHORS, INCLUDING:

Daniel N Wilson
Ludwig-Maximilians-University of Munich
148 PUBLICATIONS **4,701** CITATIONS
SEE PROFILE

Knud H Nierhaus
Charité Universitätsmedizin Berlin
348 PUBLICATIONS **11,273** CITATIONS
SEE PROFILE

Barry Cooperman
University of Pennsylvania
259 PUBLICATIONS **6,264** CITATIONS
SEE PROFILE

EF-G-Dependent GTPase on the Ribosome. Conformational Change and Fusidic Acid Inhibition†

Hyuk-Soo Seo,‡,§ Sameem Abedin,‡ Detlev Kamp,|| Daniel N. Wilson,|| Knud H. Nierhaus,|| and Barry S. Cooperman*,‡

Department of Chemistry, University of Pennsylvania, Philadelphia, Pennsylvania 19104-6323, and Max-Planck Institute for Molecular Genetics Berlin-Dahlem, 14195 Berlin, Germany

Received August 22, 2005; Revised Manuscript Received December 16, 2005

ABSTRACT: Protein synthesis studies increasingly focus on delineating the nature of conformational changes occurring as the ribosome exerts its catalytic functions. Here, we use FRET to examine such changes during single-turnover EF-G-dependent GTPase on vacant ribosomes and to elucidate the mechanism by which fusidic acid (FA) inhibits multiple-turnover EF-G·GTPase. Our measurements focus on the distance between the G′ region of EF-G and the N-terminal region of L11 (L11-NTD), located within the GTPase activation center of the ribosome. We demonstrate that single-turnover ribosome-dependent EF-G GTPase proceeds according to a kinetic scheme in which rapid G′ to L11-NTD movement requires prior GTP hydrolysis and, via branching pathways, either precedes P_i release (major pathway) or occurs simultaneously with it (minor pathway). Such movement retards P_i release, with the result that P_i release is essentially rate-determining in single-turnover GTPase. This is the most significant difference between the EF-G· GTPase activities of vacant and translocating ribosomes [Savelsbergh, A., Katunin, V. I., Mohr, D., Peske, F., Rodnina, M. V., and Wintermeyer, W. (2003) *Mol. Cell 11*, 1517−1523], which are otherwise quite similar. Both the G′ to L11-NTD movement and P_i release are strongly inhibited by thiostrepton but not by FA. Contrary to the standard view that FA permits only a single round of GTP hydrolysis [Bodley, J. W., Zieve, F. J., and Lin, L. (1970) *J. Biol. Chem. 245*, 5662−5667], we find that FA functions rather as a slow inhibitor of EF-G·GTPase, permitting a number of GTPase turnovers prior to complete inhibition while inducing a closer approach of EF-G to the GAC than is seen during normal turnover.

The ribosome is a large ribonucleoprotein particle responsible for protein synthesis in all living organisms, a complex process involving many auxiliary protein factors. With the basic structure of the bacterial ribosome now known (*1*−*6*), protein synthesis studies are increasingly focusing on delineating the nature of conformational changes that occur as the ribosome exerts its catalytic functions. One such function is the elongation factor G (EF-G)[1]-dependent hydrolysis of GTP, and it is this process that we address in the paper presented herein.

EF-G catalyzes the translocation of the ribosome by one codon relative to mRNA and the concomitant movement of the A- and P-site tRNAs, in a process that is coupled to GTP hydrolysis. Such hydrolysis is mediated by the EF-G interaction with the so-called "GTPase activation center" (GAC), which contains ribosomal protein L11 and a highly conserved 58-nucleotide stretch of 23S ribosomal RNA (rRNA) nucleotides (1051−1108 in *Escherichia coli*; *7*, *8*). Cryoelectron microscopy (cryo-EM) studies have indicated that both EF-G·GTP binding to ribosomes and subsequent GTP hydrolysis are accompanied by large structural changes in the ribosome (*9*, *10*). In these earlier studies, the ribosome·EF-G·GDPCP complex, containing the nonhydrolyzable analogue GDPCP and denoted complex 1, was used as a model for the ribosome·EF-G·GTP complex. The ribosome·EF-G·GDP complex formed in the presence of fusidic acid (FA) was used as a model for the complex following GTP hydrolysis and is denoted complex 2. FA acts by stabilizing EF-G·GDP binding to the ribosome (*11*). Formation of complex 1 involves a ratchet-like rotation of the 30S subunit with respect to the 50S subunit in response to EF-G·GDPCP binding (*12*). This ratchet movement is partially reversed in complex 2. In addition, an arc-like structure is seen in complex 2, which has been interpreted as being formed by a movement of the G′ domain of ribosome-bound EF-G

† This work is supported by NIH Grant GM 071014 (to B.S.C.) and by DFG Grant NI 174/8-1, 2, and 3 (to K.H.N.).

* To whom correspondence should be addressed: Department of Chemistry, University of Pennsylvania, Philadelphia, PA 19104-6323. Telephone: 215-898-6330. Fax: 215-898-2037. E-mail: cooprman@pobox.upenn.edu.

‡ University of Pennsylvania.

§ Current address: Laboratory of Cell Biology, Rockefeller University, New York, NY 10021-6399.

|| Max-Planck Institute for Molecular Genetics Berlin-Dahlem.

[1] Abbreviations: CPM, 7-diethylamino-3-(4′-maleimidylphenyl)-4-methylcoumarin; EF-G, elongation factor G; EF-G^F and EF-G^{C1}, EF-G labeled at position 216 with either fluorescein or CPM, respectively; FRET, fluorescence resonance energy transfer; FA, fusidic acid; GAC, GTPase activation center; IAF, 5-iodoacetamido-fluorescein; $L11^{C2}$, ribosomal protein L11 labeled with MDCC at position 38; MDCC, 7-diethylamino-3-((((2-maleimidyl)ethyl)amino)carbonyl)coumarin; NTD, N-terminal domain, PBP, phosphate-binding protein, PBP^{C2}, PBP labeled with MDCC, ThS, thiostrepton.

10.1021/bi0516677 CCC: $33.50
Published on Web 02/01/2006

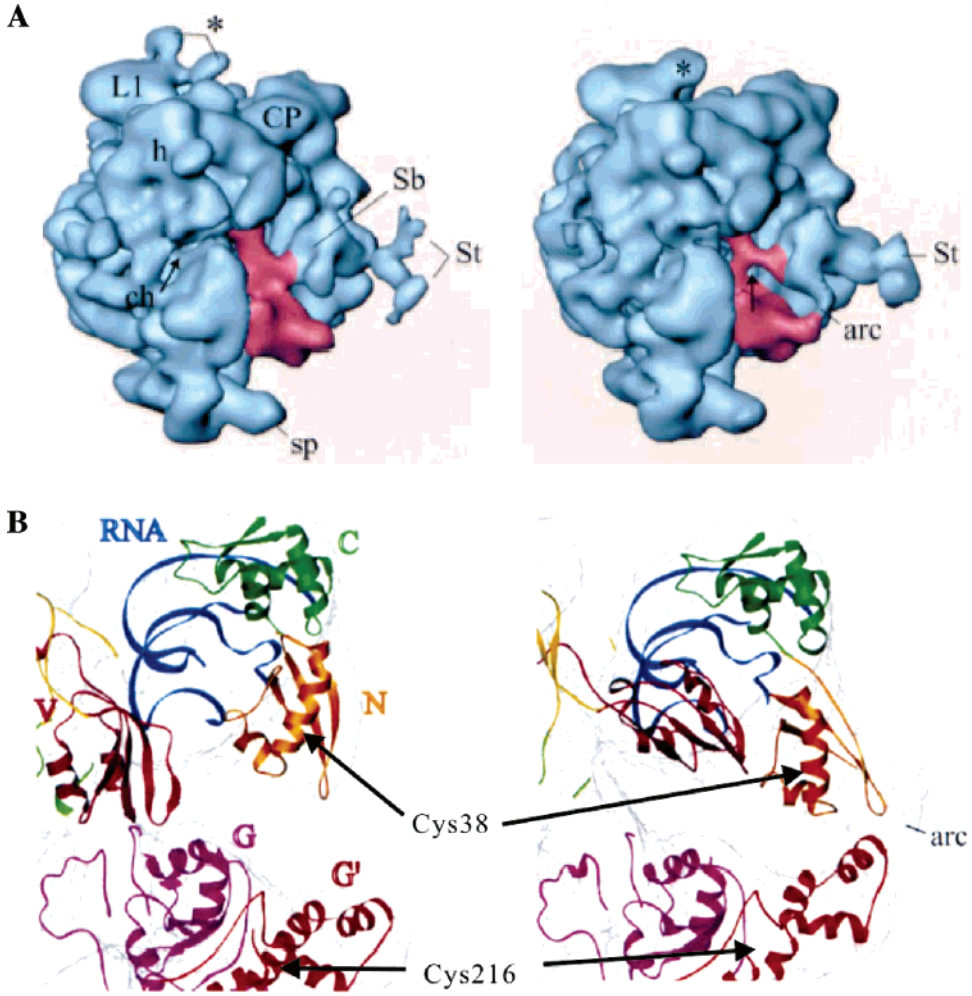

FIGURE 1: G → L11-NTD movement. (Left) Complex 1, 70S·EF-G·GDPCP; (right) complex 2, 70S·$(tRNA)_2$EF-G·GDP·FA (adapted from ref *10*). (A) Entire 70S ribosome. The position of bound EF-G is indicated in red. Landmarks of the 50 S subunit: L1, protein L1; St, stalk; Sb, stalk base; arc, arc-like connection. Landmarks of the 30 S subunit: h, head; sp, spur; ch, mRNA channel. (B) Detail showing N-terminal (N) and C-terminal (C) portions of L11 and G and G′ regions of EF-G. The positions of L11 residue 38 and EF-G residue 216 are indicated. The position and inferred conformation of EF-G are the same when tRNA is omitted from complex 2 (*9*).

toward the N-terminal region of L11 (L11-NTD) (*10*) (Figure 1).

Here, we use both static and stopped-flow fluorescence resonance energy transfer (FRET) experiments to examine whether the predicted G′ to L11-NTD movement occurs and, if so, how the timing of such movement compares to those of the reactions taking place during uncoupled EF-G-dependent GTPase on the ribosome, including EF-G binding, GTP hydrolysis, and P_i release. These studies permit us to present a quantitative model for single turnover of EF-G GTPase. They also provide a framework for examining the effects on the overall process of both FA and another antibiotic, thiostrepton (ThS), which binds to the GAC and interferes not only with the EF-G interaction with the ribosome (*13*−*16*) but also with both EF-G-dependent and EF-G-independent translocation (*17*, *18*).

MATERIALS AND METHODS

Except as specified below, materials were obtained and methods were performed as described elsewhere (*19*−*21*). 5-Iodoacetamido-fluorescein (IAF), 7-diethylamino-3-((((2-maleimidyl)ethyl)amino)carbonyl)coumarin (MDCC), and 7-diethylamino-3-(4′-maleimidylphenyl)-4-methylcoumarin (CPM) were obtained from Molecular Probes.

Buffers. pH values were determined at 25 °C. W buffer ($T_{50}A_{30}K_{70}M_7D_1$), 50 mM Tris at pH 7.6, 30 mM NH_4Cl, 70 mM KCl, 7 mM $MgCl_2$, and 1 mM DTT; L11 storage buffer ($H_{20}A_{400}M_{20}E_1SH_4$), 20 mM HEPES at pH 7.6, 400 mM NH_4Cl, 20 mM $MgCl_2$, 1 mM EDTA, and 4 mM 2-mercaptoethanol; L11-labeling buffer ($H_{20}A_{400}$), 20 mM HEPES at pH 7.6 and 400 mM NH_4Cl; and AM77 storage buffer ($H_{20}A_{30}M_6$), 20 mM HEPES at pH 7.6, 30 mM NH_4Cl, and 6 mM $MgCl_2$.

Ribosomes. Tight couple wild-type 70S ribosomes were isolated from MRE600 as described (*16*). Mutant ribosomes lacking L11 were isolated from *E. coli* strain AM77. Cells were grown in rich medium in the presence of 300 μg/mL rifampicin as described (*22*), and the tight couple ribosomes were purified the same as the wild type, except that the ribosome pellets were dissolved in AM77 storage buffer at the last step.

Proteins. The quadruple EF-G variant (C113D/C265A/C397S/E216C), denoted $EF\text{-}G^{216}$, was prepared and singly labeled with either IAF, giving $EF\text{-}G^{F}$, or CPM, giving $EF\text{-}G^{C1}$, as described (*16*). Purification of phosphate-binding protein (PBP) and its labeling with MDCC, giving PBP^{C2}, was performed as described (*23*), using a plasmid containing *E. coli phoS* obtained from Martin Webb (MRC National

Institute for Medical Research, The Ridgeway, London, U.K.).

The gene for L11 was amplified from *E. coli* gDNA using PCR primers (5′-AGGAATTTCATATGGCTAAGAAAG-TACAAG-3′ and 5′-TAGGGATCCATTAGTCCTCCAC-TACCAGGC-3′) that introduce *Nde*I and *Bam*HI restriction sites (underlined) and then cloned using these sites into the pET-14b vector (Novagen). Clones containing the correct sequence were transformed into the BL21(DE3)pLysS host strain, which was grown up using a protocol for cell growth that was adapted from the pET system manual (Novagen), yielding N-terminally His-tagged L11. Partial purification of denatured (8 M urea) L11 from the cell pellet was carried out using stepwise elution from Ni-NTA agarose (Qiagen), as described in the handbook of the manufacturer. SDS−PAGE analysis of the pooled fractions showed L11 to be the dominant protein, contaminated with two higher molecular-weight proteins. The sample was concentrated (Centricon YM-10), exchanged into the renaturing $H_{20}A_{400}$ buffer using a PD-10 column at a concentration of ∼100 μM L11, and reacted at 37 °C with a 0.1 volume of 10.4 mM MDCC in DMF, added dropwise with stirring. After incubation for 40 min at 37 °C, the reaction was quenched with 2-mercaptoethanol and excess reagent was removed by a combination of gel and Centricon-10 filtration. All three proteins in partly purified L11 were labeled with MDCC by this procedure, as shown by SDS−PAGE analysis and fluorescence detection. This preparation is denoted pp$L11^{C2}$.

Reconstituted Ribosomes. In a typical preparation of ribosomes containing MDCC-labeled L11 (denoted $70S^{C2}$), pp$L11^{C2}$ (27 nmol of coumarin dye) was incubated with 6 nmol of AM77 ribosomes in 450 μL of W buffer for 20 min at 44 °C. Excess dye was removed by centrifugation (40 000 rpm; Ti 70.1 rotor; 20 h) through a sucrose cushion (1.1 M sucrose in W buffer), yielding a ribosome pellet with an MDCC/ribosome ratio of 0.97−1.02/1. SDS−PAGE analysis of the protein fraction of the reconstituted AM77 ribosome showed it to contain a single fluorescent band, corresponding to L11 labeled at its unique Cys residue (position 38), i.e., $L11^{C2}$. Thus, the AM77 ribosome selectively takes up $L11^{C2}$ from the mixture of fluorescent proteins present in pp$L11^{C2}$ in a stoichiometry of 1 $L11^{C2}$/ribosome, yielding $70S^{C2}$, which was fully active in poly(U)-dependent polyPhe synthesis. A control reconstitution experiment performed with wild-type MRE 600 ribosomes resulted in an MDCC/ribosome ratio of <0.1.

In an analogous experiment, a more nearly homogeneous L11 sample (∼0.09 mg) was reacted with *tert*-butoxycarbonyl-L-[^{35}S]methionine-*N*-hydroxysuccinimidyl ester (Amersham, 200 pmol) in 200 μL of labeling buffer (0.1 M borate buffer at pH 8.4 and 0.4 M NH_4Cl) for 60 min on ice with stirring, followed by quenching with 300 μL of 0.2 M glycine solution in 0.1 M borate buffer (pH 8.4). Excess reagent was removed by gel filtration, yielding a labeled protein with a specific activity of 15.3 cpm/pmol. Reconstitution with AM77 ribosomes (30 pmol) proceeded as above, with unbound ^{35}S-labeled L11 removed by gel filtration. Incorporation reached a plateau level of 0.94 ^{35}S-labeled L11/ribosome as a function of added ^{35}S-labeled L11 (15−75 pmol).

Adding His-tagged L11 to AM77 ribosomes (a) protects A1088, A1089, and A1095 from dimethyl sulfate modification, as shown by the primer extension assay (*19*) using the oligodeoxynucleotide complementary to 23S nucleotides 1140−1156 as primers, in agreement with previous findings using native *E. coli* L11 (*24*), and with a crystal structure showing that A1088 and A1095 make strong contacts with the C-terminal domain of L11 (*8*) and (b) induces (p)ppGpp synthesis, which is totally dependent upon the presence of a functional L11 (*25*). These results strongly suggest that His-tagged L11 binds to the normal L11 site within the 50S subunit.

Equilibrium and Kinetic Measurements. All equilibrium and kinetic experiments were performed at 25 °C. Samples were prepared on ice in W buffer and incubated for 15 min at 37 °C followed by incubation for at least 10 min at 25 °C prior to measurement. All concentrations specified in the text and figure captions refer to final concentrations after mixing.

Equilibrium Fluorescence. Solutions containing $70S^{C2}$ were excited at 425 nm, and emission was monitored from 440 to 600 nm (SPEX Fluorolog-3, Jobin Yvon, Inc.)

Stopped-Flow Fluorescence. Emission traces were acquired using an Applied Photophysics SX.18MV stopped-flow spectrofluorometer. Excitation was at 436 nm for solutions containing either $70S^{C2}$ and/or $EF\text{-}G^{F}$ or PBP^{C2} using an Hg−Xe lamp (Hamamatsu Corp., Bridgewater, NJ) and at 395 nm for solutions containing $EF\text{-}G^{C1}$. Emission was monitored at either 470 nm, using a second monochromator (FRET donor fluorescence), or at 520 nm, using either an interference filter (FRET acceptor fluorescence, 10 nm bandwidth, Thermo Oriel) or a 455 nm cutoff filter ($EF\text{-}G^{C1}$ and PBP^{C2}). Slit widths were set at 2 mm (excitation) and 6 mm (emission) when the second monochromator was used or at 0.5 mm (excitation) when either the 520 nm interference filter or 455 nm cutoff filter was used. At least three independent fluorescence traces were averaged for each reported result.

P_i Release. All solutions contained the enzymatic cleanup system ["P_i mop", purine nucleoside phosphorylase (1 unit/mL) and 7-methylguanosine (750 μM) (*23*)] to minimize P_i contamination. In addition, the syringes, tubing, and cell were preincubated with a buffer containing "P_i mop" for at least 10 min prior to measurement. The voltage change in the stopped-flow spectrophotometer was linear with [P_i] until the P_i concentration approached that of PBP^{C2}, permitting accurate estimation of the stoichiometry of rapid P_i release during the stopped-flow experiment ($t \leq \sim 1.5$ s) and allowing the P_i release data to be fit directly to Scheme 1. At longer times, removal of PBP^{C2}-bound P_i by "P_i mop" becomes significant, so that fluorescence change no longer provides an accurate measure of P_i release.

GTP Hydrolysis. Quenched-flow kinetic studies were carried out using a KinTek Chemical-Quench-Flow Model RQF-3 machine. After rapid mixing of the ribosome and EF-G·[γ-^{32}P]GTP solutions and incubation for the desired reaction time, the reaction was quenched by 0.6 M $HClO_4$ and 1.8 mM potassium phosphate and quick-frozen. Multiple-turnover GTPase was carried out similarly, using hand mixing. $^{32}P_i$ was extracted into isopropyl acetate as a dodecamolybdate complex (*26*), and the radioactivity of the organic phase was determined.

Rate Constant Determination: Global Fitting. Global fitting to Scheme 1 of the data presented in Figures 3B, 4A, 5, and 6B was carried out using the program Scientist

(MicroMath Research, LC). Choices of initial values of k_1, k_{-1}, $k_2 + k_{-2}$ (122 s^{-1}), and $k_3 + k_{-3}$ (40 s^{-1}) and for the net rate constant for the overall reaction including regeneration of ribosome•EF-G•GTP from ribosome•EF-G•GDP (via steps 7, 8, and 1 or via step 7′) came directly from results presented in Figures 4 and 5. With these initial values set, values of k_{-2}, k_{-3}, k_4/k_5, and k_6 were fit iteratively to the P_i release data (Figure 6B) by alternatively holding k_{-2}, k_{-3}, or k_4/k_5 and k_6 constant until a best fit was achieved. Subsequent refitting of rate constants k_1, k_{-1}, k_2, k_{-2}, k_3, and k_{-3} using the results presented in Figure 3B, as well as Figures 4 and 5, led to at most minor changes from initial values. In all fittings of fluorescence data, the traces of samples containing the same concentrations of nonfluorescently labeled components were used as a background and subtracted from traces containing fluorescently labeled components.

FRET Efficiency and Distance Calculations. Distances between the fluorophores $70S^{C2}$ (donor) and EF-G^F (acceptor) were calculated from eq 1 (*27*).

$$R = R_o\left(\frac{1}{E} - 1\right)^{1/6} \tag{1}$$

The Förster distance R_o was calculated from eq 2, where ϕ_D is the quantum yield of $70S^{C2}$, η is the refractive index of water (=1.33; *28*), κ^2 is a dipole orientation factor and was set equal to $^2/_3$ assuming random orientations of the fluorophores (*27*), and $J(\lambda)$ is the spectral overlap integral. ϕ_D was determined by comparing the integrated fluorescence of $70S^{C2}$ to that of a standard, Coumarin 6 (Exciton, Dayton, OH; *29*), as described (*27*), yielding a value of 0.51 ± 0.03. $J(\lambda)$, equal to 1.58×10^{-13} M^{-1} cm^3, was determined from the fluorescence and absorption spectra of $70S^{C2}$ and EF-G^F, respectively (*30*). These values permit the calculation of R_o equal to 50 ± 1 Å, in good agreement with other reported values of 47−52 Å for the coumarin/fluorescein pair (*31*, *32*).

$$R_o\,(\text{Å}) = [8.8 \times 10^{-5} \cdot \kappa^2 \cdot \eta^{-4} \cdot \phi_D \cdot J(\lambda)]^{1/6} \tag{2}$$

The efficiency of energy transfer, E, was determined by both a donor fluorescence decrease at 470 nm and an acceptor fluorescence enhancement at 520 nm. Measurements were made in parallel on the DA (donor + acceptor), D (donor only), and A (acceptor only) samples for each ribosome complex (equilibrium experiments) or kinetic process (stopped-flow experiments). The signal for the corresponding blank sample containing unlabeled ribosomes and EF-G was subtracted from each of the D, DA, and A samples to correct for light scattering and background fluorescence. Small corrections were made for the optical inner filtering effect as described (*16*).

Equilibrium Measurements. Donor fluorescence at 470 nm has no contribution from the acceptor, permitting E to be calculated from the fluorescence intensities measured for the DA and D samples, corrected for the fraction of ribosomes containing bound EF-G. These corrected values, designated $F^c_{DA}(\lambda_D)$ and $F^c_D(\lambda_D)$, are calculated from the measured F_{DA} and F_D values from eqs 3 and 4, where R and RG refer to free and EF-G-bound ribosomes, respectively, $[R]_T$ is the total ribosome concentration, and $F_{D,f}$ is the apparent fluorescence of unbound ribosomes. Values of [R] and [RG] were calculated using K_d values of 0.05 μM for complex 1 (*16*) and 0.03 μM for complex 2 (*33*). E was calculated from eq 5.

$$F^c_{DA} = \frac{F_{DA}[R]_T - F_{D,f}[R]}{[RG]} \tag{3}$$

$$F^c_D = \frac{F_D[R]_T - F_{D,f}[R]}{[RG]} \tag{4}$$

$$E = \left(1 - \frac{F^c_{DA}(\lambda_D)}{F^c_D(\lambda_D)}\right) \tag{5}$$

Calculation of acceptor fluorescence enhancement required two steps. First, subtraction of the fitted donor contribution to 520 nm fluorescence, calculated from the intensity of the 470 nm fluorescence in the DA sample and the 520:470 ratio of fluorescence intensities for the D sample, which yielded the extracted acceptor emission. Second, correction for the fraction of EF-G bound to ribosomes, calculated in a manner similar to that described above. The resulting corrected values, denoted $F^{*c}_{DA}(\lambda_A)$ and $F^{*c}_A(\lambda_A)$ were used to calculate E from eq 6.

$$E = \left(\frac{\epsilon_A(\lambda_{ex})}{\epsilon_D(\lambda_{ex})}\right)\left(\frac{F^{*c}_{DA}(\lambda_A)}{F^{*c}_A(\lambda_A)}\right) \tag{6}$$

Fluorescence Parameters from Stopped-Flow Studies. ϕ values, corresponding to the specific relative fluorescences of all fluorescent species present in solution, were determined for EF-G^{C1}•GTP binding (Figure 4) and for FRET results (Figure 3B, donor decrease), through fitting of the data obtained to eqs 7 and 8, respectively, using the program Scientist, with [I] values as a function of the time determined using the rate constants in Scheme 1. Because $F_D(t)$ was unchanged over the course of the stopped-flow experiment, changes in the ratio in eq 8 directly reflect changes in the DA sample.

$$F(t) = \sum_i \phi_i[I] \tag{7}$$

$$\frac{F_{DA}(t)}{F_D(t)} = \frac{\sum_i \phi_i^{DA}[I]}{\sum_i \phi_i^{D}[I]} \tag{8}$$

Apparent Rate Constants. Biphasic fluorescent changes were fit to eq 9 to generate values of $k_{app,1}$ and $k_{app,2}$.

$$F(t) = F_o + \Delta F_1 e^{-k_{app,1}t} + \Delta F_2 e^{-k_{app,2}t} \tag{9}$$

RESULTS

Equilibrium FRET Measurements and Dye−Dye Distances. Equilibrium FRET experiments were carried out using an EF-G variant derivatized with a fluorescein acceptor dye (A) at position 216, denoted EF-G^F, and 70S ribosomes containing a coumarin donor dye (D) uniquely placed on Cys 38 of protein L11, denoted $70S^{C2}$. Energy transfer was measured from $70S^{C2}$ to EF-G^F in complexes 1 and 2 (Figure

2). From the results, it is clear that both the decrease in donor fluorescence (ΔD) and the increase in acceptor fluorescence (ΔA) is greater in complex 2 than in complex 1. The corrected fluorescence intensities of the donor in the DA samples relative to the D samples and of the acceptor in the DA samples relative to the A samples allow for the calculation of energy-transfer efficiencies and dye−dye distances, which are 65.3 ± 1.6 and 59.9 ± 0.7 Å for complexes 1 and 2, respectively.

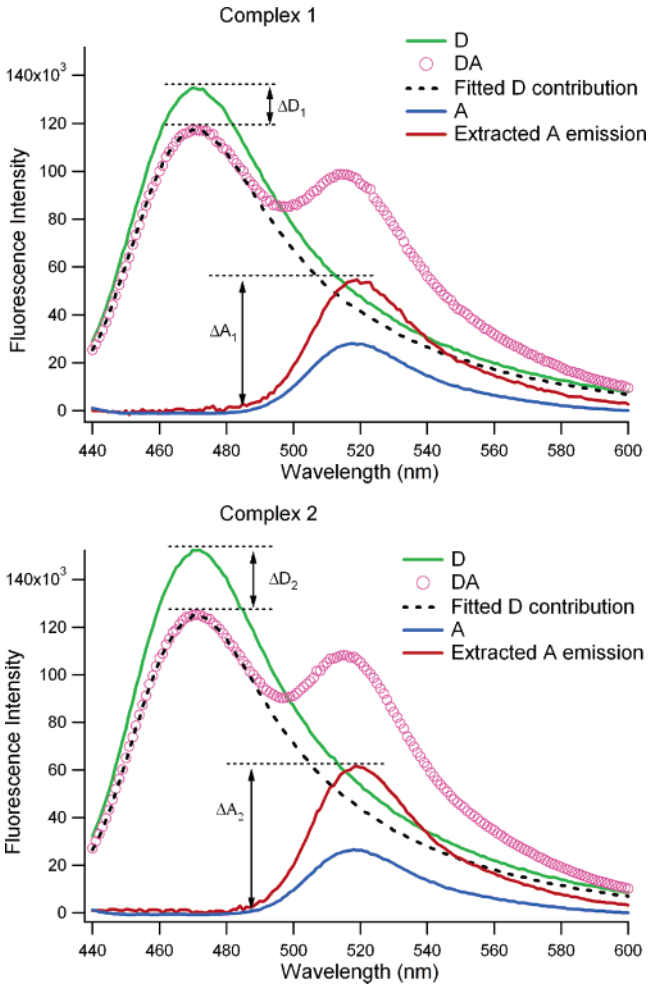

FIGURE 2: FRET in complex 1, 70S·EF-G·GDPCP, and complex 2, 70S·EF-G·GDP·FA. Samples were prepared at 26 ± 2 °C in W buffer and contained 70S ribosomes (0.5 μM), EF-G (0.75 μM), and either 100 μM of GDPCP (complex 1) or 100 μM GTP and 50 μM FA (complex 2). DA samples contain $70S^{C2}$ and $EF\text{-}G^{F}$; D samples contain $70S^{C2}$ and $EF\text{-}G^{216}$; and A samples contain 70S and $EF\text{-}G^{F}$. Excitation was at 425 nm. The fitted donor contribution and extracted acceptor emission are defined in the Materials and Methods.

Kinetics of FRET Change. Rapid FRET change was used to monitor G′ to L11-NTD movement during the course of single turnover, EF-G·GTPase on the ribosome (0.0−0.3 s), measuring either the decrease at 470 nm (donor maximum, trace 2 in Figure 3A) or the increase at 520 nm (acceptor maximum, trace 4 in Figure 3A). Both changes occur at the same rates. Measurement of the apparent rate constant for the rapid decrease in donor absorbance at 470 nm as a function of the increasing $EF\text{-}G^{F}$ concentration (Figure 3B) allows for an estimation of a saturated value for the rate constant of 24 ± 3 s^{-1}.

Substitution of GDPCP for GTP leads to virtually a complete loss of rapid FRET change (Figure 3C). However, observed over a much longer time scale (0−100 s, Figure 3D), it is clear that the overall FRET change measured in the presence of either GTP or GDPCP is of similar magnitude. For the results presented in Figure 3D, measured at 0.75 μM EF-G, the FRET change in the presence of GTP is biphasic and was fit to a double exponential (eq 9), with $k_{app,1}$ and $k_{app,2}$ values of 20 ± 3 and 0.23 ± 0.02 s^{-1}, respectively, with the larger change occurring in the first phase of the reaction. The FRET change in the presence of GDPCP is also biphasic but proceeds much more slowly, with $k_{app,1}$ and $k_{app,2}$ values of 0.20 ± 0.01 and 0.007 ± 0.001 s^{-1}, respectively, and the larger change occurring in the second phase of the reaction.

Kinetics of EF-G·GTP Binding. The kinetics of EF-G·GTP binding to the ribosome was measured by the fluorescence changes observed following the addition to ribosomes of EF-G derivatized with a coumarin at position 216, denoted $EF\text{-}G^{C1}$. The biphasic kinetic traces observed, in which a rapid decrease is followed by a somewhat slower increase (Figure 4A) are quite similar in both rate and magnitude to what was observed previously for $EF\text{-}G^{C1}$·GDPCP (*16*). The traces obtained over a range of ribosome concentrations were each fit to eq 9 (Figure 4B). $k_{app,1}$ is linearly dependent upon the ribosome concentration, indicating that it measures $EF\text{-}G^{C1}$·GTP binding. From the slope and the intercept of the linear fit, $k_{binding} = 35 \pm 5\ \mu M^{-1}\ s^{-1}$ and $k_{dissociation} = 25 \pm 10\ s^{-1}$. $k_{app,2}$ (∼26 ± 2 s^{-1}) is independent of the ribosome concentration, corresponds to a conformational change step, and is indistinguishable from the value determined above for rapid FRET change.

Kinetics of EF-G·GTP Hydrolysis. Quenched-flow data measuring single-turnover GTP hydrolysis (≤0.1 s) as a function of the EF-G concentration are shown in parts A−D of Figure 5. Essentially identical results were obtained when $70S^{C2}$ ribosomes replaced MRE600 ribosomes and 0.75 μM $EF\text{-}G^{F}$ replaced 0.75 μM EF-G (data not shown). The curves obtained are biphasic, with an initial burst followed by a much slower release, corresponding to the steady-state rate of multiple-turnover GTP hydrolysis. The extrapolated burst height shows only a weak dependence on [EF-G] in the range measured, ranging from 0.74/ribosome at 0.75 μM EF-G to 0.90/ribosome at 5.0 μM EF-G. While the latter value indicates the possibility of appreciable reversibility of the GTP hydrolysis within the ribosome.EF-G complex, it does not establish this point unambiguously, because the small difference from unity could be due to a minor fraction of the EF-G preparation being inactive in GTP turnover.

The burst phase could be fit with a single apparent rate constant for each concentration of EF-G employed, yielding a saturated rate constant for single-turnover GTPase of 122 ± 23 s^{-1} and an apparent K_M of 2.6 ± 0.9 μM (Figure 5E). In comparison, the measurement of the steady-state multiple-turnover GTPase rate as a function of the EF-G concentration gives values for k_{cat} and K_m of 4.3 ± 0.3 s^{-1} and 1.4 ± 0.3 μM, respectively (Figure 5F).

Kinetics of P_i Release. The release of P_i following GTP hydrolysis proceeds in three distinct phases (Figure 6A); a lag phase (∼0.03 s), followed by a burst of release, but with a stoichiometry considerably less than 1 equiv/ribosome, and third, a linear portion (>0.1 s) proceeding at a slower rate

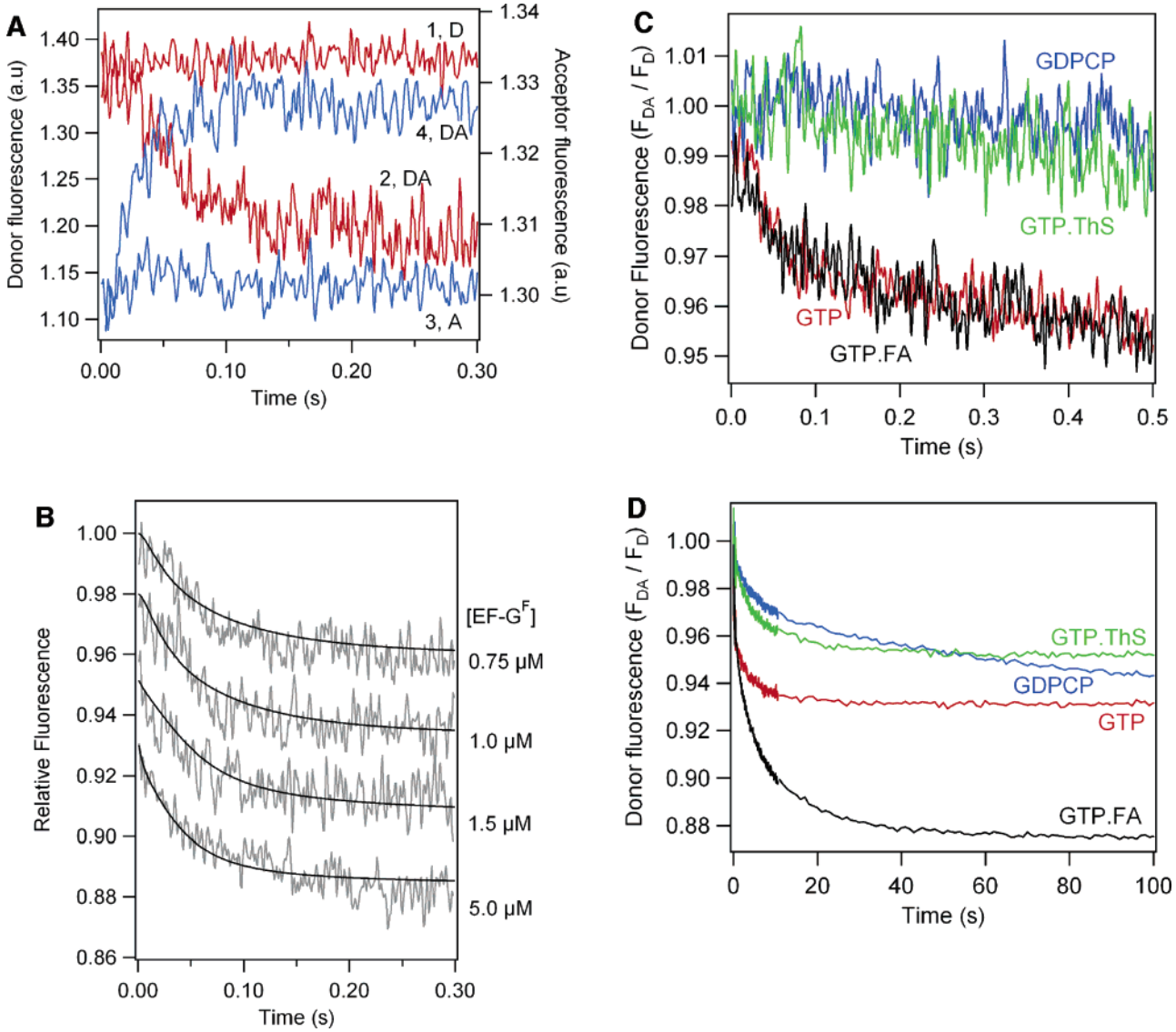

FIGURE 3: Kinetics of FRET change. 70S ribosomes were rapidly mixed with EF-G and G nucleotide at 25 °C, and fluorescence was monitored. Excitation was at 436 nm. In all experiments, the final concentrations, except as otherwise indicated, were ribosomes, 0.5 μM; EF-G, 0.75 μM; and GTP or GDPCP, 100 μM. (A) DA sample, 70S^{C2} and EF-G^{F} monitored at either 470 nm (trace 2) or 520 nm (trace 4); D sample, 70S^{C2} and unlabeled EF-G monitored at 470 nm (trace 1); A sample, 70S and EF-G^{F} monitored at 520 nm (trace 3). (B) Dependence of the rate of rapid FRET change on EF-G^{F} (final concentrations of 0.75−5 μM), as monitored by relative donor fluorescence (470 nm). The curves are fits to Scheme 1 and are offset by 0.02 unit relative to one another for clarity. (C) Effects of ThS or FA or GDPCP replacement of GTP on the rate of relative donor fluorescence decrease (470 nm). (Red trace) As in A, trace 2. (Green trace) 70S^{C2} was preincubated for 15 min with ThS (5 μM final concentration). (Black trace) 70S^{C2} was preincubated for 15 min with FA (50 μM final concentration). (Blue trace) GDPCP replaced GTP. (D) Kinetics of slow FRET change. The color coding of the four traces is the same as in C: red, GTP, no antibiotic; green, GTP, preincubation with ThS; black, GTP, preincubation with FA; blue, GDPCP replaces GTP, no antibiotic. Donor fluorescence was monitored at 470 nm. Final concentrations were ThS (5 μM) and FA (50 μM). For the FA and GDPCP samples, the decreases in donor fluorescence are closely matched by corresponding increases in acceptor fluorescence.

and continuing into the steady state for multiple turnover. The rates of each of the three phases increase as [EF-G] is increased (Figure 6B).

Placing the Rapid FRET Change Step within an Overall Scheme for EF-G·GTPase on the Ribosome. The kinetic measurements of EF-G binding, single- and multiple-turnover GTPase, and P_i release were used to formulate and estimate rate constants for a minimal reaction scheme describing single-turnover EF-G GTPase on the ribosome (Scheme 1). A direct comparison of the four rapid kinetic measures of the EF-G·GTP interaction with the ribosome reported in this paper is provided in Figure 7.

The first two steps in Scheme 1 were assigned to EF-G·GTP binding (step 1), measured by the initial phase of the change in fluorescence following the addition of EF-G^{C1}·GTP to the ribosome (Figure 4), and subsequent GTP hydrolysis (step 2). Both reactions 2 and 3 were fitted as reversible steps. However, the low values of the estimated reverse constants show these back reactions to be relatively inconsequential. In fact, although fits obtained setting both k_{-2} and k_{-3} to 0 were distinctly worse, setting either rate constant to 0 had only a minor effect. The low stoichiometry of the burst phase of P_i release (Figure 6) necessitates the branching seen in steps 4 and 5.

Rapid FRET change (Figure 3A) and the second phase of fluorescence change following the addition of EF-G^{C1} to the ribosome (Figure 4) provide measures of conformational change during single turnover that proceed with essentially

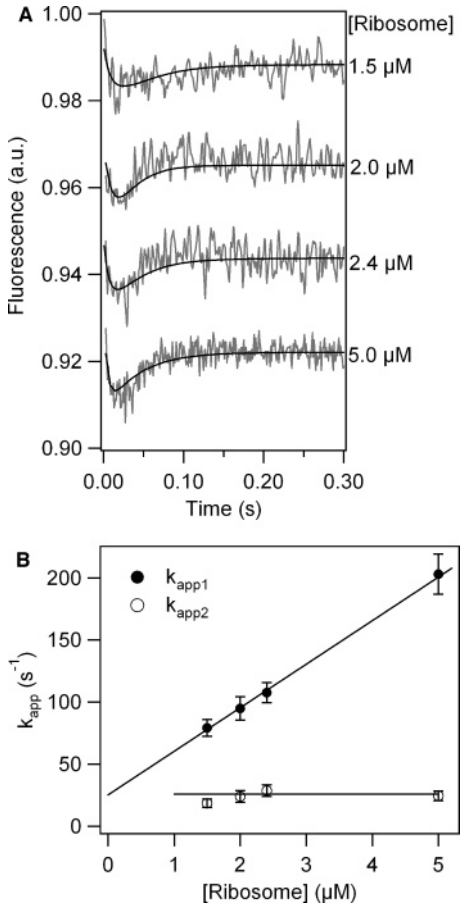

FIGURE 4: Kinetics of EF-G^{C1}·GTP binding to the ribosome. 70S ribosomes were rapidly mixed with EF-G^{C1} in the presence of GTP, and emission from 395 nm excitation was recorded using a 455 nm cutoff filter. Final concentrations were 70S, 1.5−5 μM; EF-G^{C1}, 0.1 μM; and GTP, 100 μM. The curves are fits to Scheme 1. No further changes in EF-G^{C1} fluorescence were seen for periods of up to 5.5 s. (B) Dependence of apparent rate constants (eq 9) on the ribosome concentration.

identical apparent rate constants in the presence of GTP. However, substitution of GDPCP for GTP, while having almost no effect on the rate of the latter change (this paper and ref *16*), leads to a much reduced rate of rapid FRET change (Figure 3C). Thus, the two measures of conformational change must be monitoring different processes, while sharing a common rate-determining step in the presence of GTP.

Scheme 1 incorporates this conclusion by positing a sequence of two conformational changes, state a → state b and state b → state c. Here, the first conformational change (step 3) is monitored by the change in EF-G^{C1} fluorescence and is rate-determining in the presence of GTP, while the second conformational change is monitored by the FRET change and either precedes P_i release (steps 4 and 6) or occurs so rapidly after P_i release that it is essentially simultaneous with it (step 5).

Multiple-turnover GTPase on vacant ribosomes requires the regeneration of ribosome·EF-G·GTP from ribosome·EF-G·GDP. Two alternatives are presented, reflecting our present inability to choose between regeneration via steps 7, 8, and 1 (part 1 in Scheme 1) or via direct nucleotide exchange on ribosome·EF-G·GDP to form ribosome·EF-G·GTP (step 7′) (part 1a in Scheme 1). In fact, there is evidence that each of these alternatives is possible (*34*, *35*).

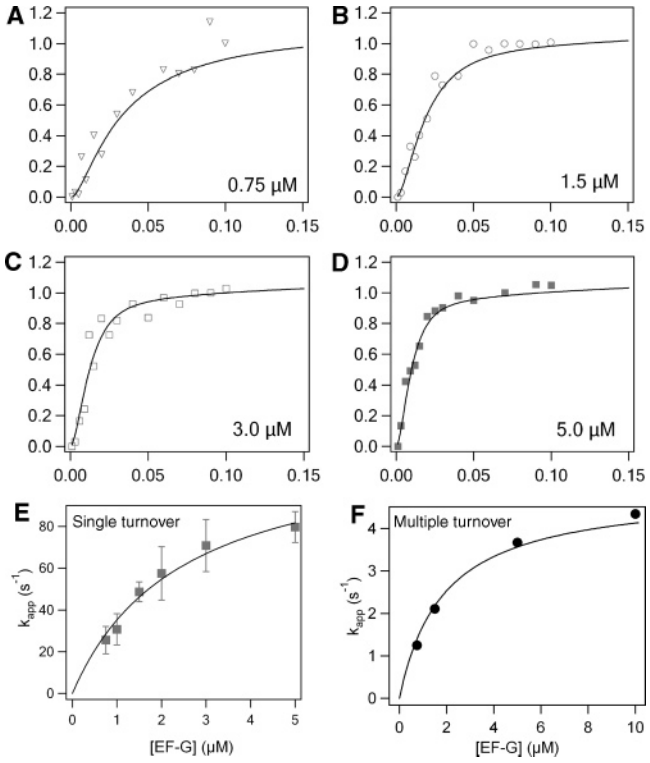

FIGURE 5: GTPase kinetics. (A−D) Sample data for single-turnover GTPase measured on rapid mixing of ribosomes with EF-G and GTP. Final concentrations were ribosomes, 0.5 μM; EF-G, 0.75−5.0 μM as indicated; and [γ-^{32}P]GTP, 25 μM. Solid lines are fit to Scheme 1. *y* axis, P_i formed/ribosome; *x* axis, time (s). (E and F) The dependence of k_{app} on [EF-G] for single- and multiple-turnover GTPase, respectively. Measured values are fit to $k_{app} = k_{sat}$[EF-G]/(K_m + [EF-G]). In F, final concentrations were EF-G, 0.5 μM; ribosomes, 1.0 μM; GTP, 1 mM.

The net rate constant for P_i release in Scheme 1, 5.0 ± 0.5 s^{-1}, as given by $k_6(1 + k_5/k_4)$ (*36*), clearly shows P_i release to be essentially rate-determining in single-turnover GTPase. Because this value is very close to the value of k_{cat} for multiple turnover (4.3 ± 0.3 s^{-1}), we were unable to estimate values of k_7 and k_8 (or of k_7') from the experiments presented here. However, it is clear that the GDP/GTP exchange process is rapid relative to P_i release.

Antibiotic Effects. Consistent with earlier results, ThS does not affect single-turnover GTPase (Figure 8A; *13*) but strongly inhibits both single-turnover P_i release (Figure 8B; *13*) and multiple-turnover GTPase (Figure 8C; *13*, *14*). ThS also inhibits rapid FRET change (Figure 3C). Because ThS has previously been shown to inhibit step 3 (*16*), its inhibition of rapid FRET change and P_i release (steps 4−6) is fully in accordance with Scheme 1. Interestingly, ThS does allow a slower FRET change (Figure 3D) which, although not as large as that observed in the absence of ThS, proceeds with a k_{app}, 0.23 s^{-1}, indistinguishable from that for the second phase of FRET change in the absence of added antibiotic.

FA does not affect single-turnover GTPase (Figure 8A) but, in contrast to ThS, has a comparatively modest inhibitory effect on single-turnover P_i release (Figure 8B) and only gradually brings multiple-turnover GTPase to a halt (Figure 8C). Here, preincubation of ribosomes with 100 μM FA, giving a final FA concentration of 50 μM, results in an initial rate decrease of about 4-fold and complete inhibition of GTPase after ~40 turnovers. These effects are only slightly

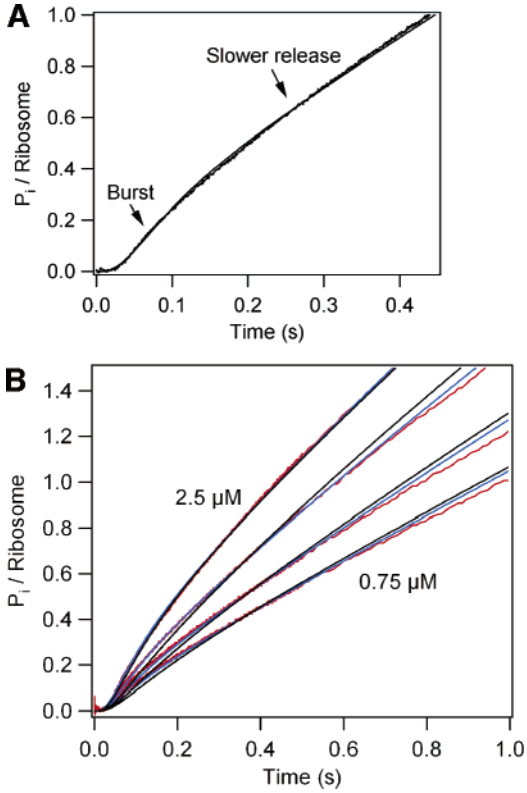

FIGURE 6: Kinetics of P_i release. 70S ribosomes (0.5 μM) were rapidly mixed with a solution containing EF-G (variable), GTP (100 μM), and PBP^{C2} (2.2 μM) at 25 °C, and emission from 436 nm excitation was recorded. All concentrations given are after mixing. (A) EF-G, 2.5 μM. The black line is fit to Scheme 1. (B) P_i release with an increasing EF-G concentration, 0.75, 1.0, 1.5, and 2.5 μM, from low to high traces. Red lines are experimental, and blue and black lines are fit to parts 1 and 1a in Scheme 1, respectively.

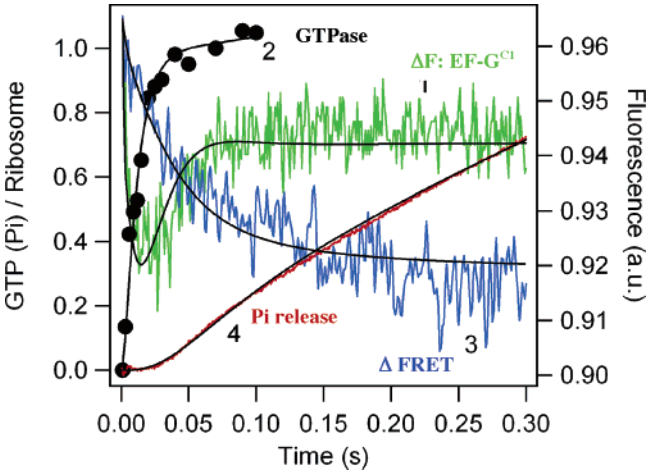

FIGURE 7: Direct comparison of rapid kinetic measures of the EF-G·GTP interaction with the ribosome. (a) EF-G^{C1} fluorescence change (trace 1), (b) GTPase (trace 2), (c) FRET change, donor fluorescence (trace 3), and (d) P_i release (trace 4). Final concentrations were EF-G, 5 μM; ribosomes 0.5 μM; GTP, 25 μM (GTPase experiment) or 100 μM (all others). Black lines through the data are fits to Scheme 1.

more marked if preincubation is conducted with EF-G rather than ribosomes but considerably more dramatic when EF-G is preincubated with a 10-fold higher FA concentration, which leads to complete inhibition after ~10 turnovers.

FA also differs from ThS in its effects on FRET change, having essentially no effect on either of the apparent rate constants for FRET change ($k_{app,1}$, 20 ± 2 s^{-1}; $k_{app,2}$, 0.23 ± 0.01 s^{-1}) or the magnitude of rapid FRET change (Figure 3C) but giving rise to a much larger FRET change in the second phase of the reaction (Figure 3D).

DISCUSSION

Comparison of FRET and Cryo-EM Results. The equilibrium FRET experiments displayed in Figure 2 are in qualitative agreement with the cryo-EM results (*10*), which have been interpreted as showing that the G′ region of EF-G is closer to L11-NTD in complex 2, the ribosome·EF-G·GDP.FA complex, than in complex 1, the ribosome·EF-G·GDPCP complex. However, the FRET estimated distances between positions 38 in L11 and 216 in EF-G, 65.3 ± 1.6 and 59.9 ± 0.7 Å for complexes 1 and 2, respectively, are somewhat larger than those calculated (α-C−α-C) for the cryo-EM structures, 45 and 37 Å (Figure 1), respectively, from coordinates deposited in the RCSB PDB (accession codes 1JQS and 1JQM). These differences could arise from several factors, including (a) the fluorophore−fluorophore distance could be considerably greater than the α-C−α-C distance, because the center of each fluorophore is ~10 Å from the corresponding α-C; (b) the PDB coordinates allowing cryo-EM-derived distance estimates are subject to considerable uncertainty; and (c) the calculated FRET distances depend upon an assumed value of the dipole orientation factor, κ^2, equal to $^2/_3$ (*27*). While there are strong arguments in favor of the latter assumption for FRET experiments of the kind presented herein (*37*, *38*), it has not been verified experimentally. Given these uncertainties, a more quantitative agreement between the two approaches would have been fortuitous.

The dynamic FRET experiments displayed in Figure 3 provide evidence for two kinetic processes, each of which

Scheme 1: EF-G-Dependent GTPase on the Ribosome (R = Ribosome and G = EF-G)[a]

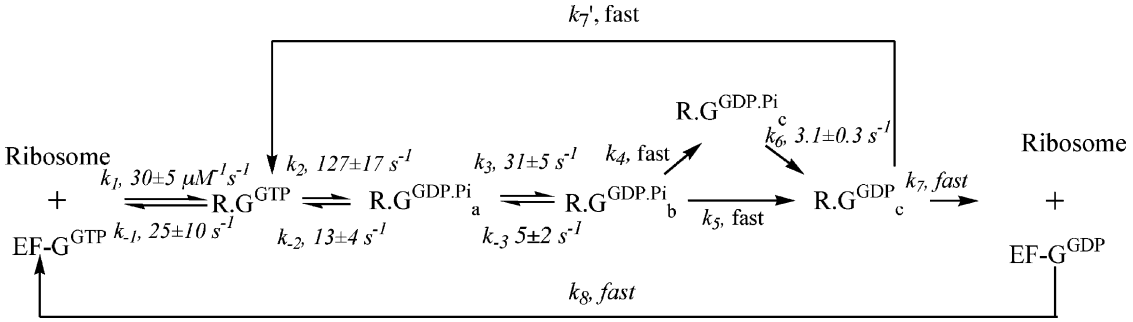

[a] Reactions 1−6 are common to both variants of the scheme, which differ only in the mechanism of GDP/GTP exchange on the ribosome: 1, via steps 7, 8, and 1; 1a, via step 7′. Although k_4 and k_5 cannot be evaluated, the ratio k_4/k_5 is best fit to a value of 1.63.

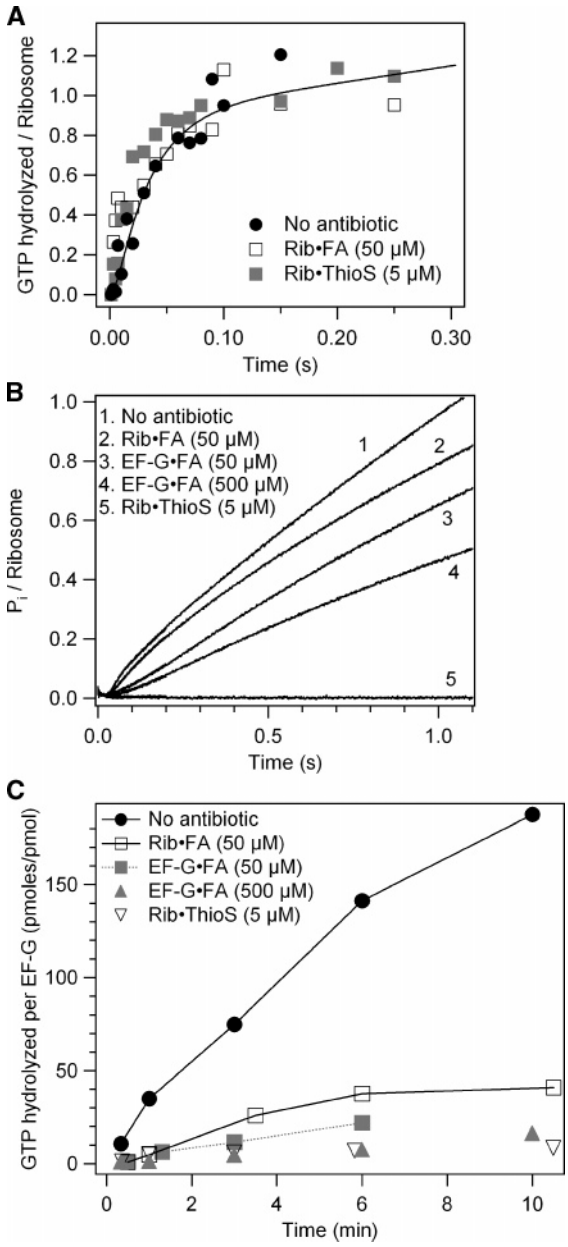

FIGURE 8: Antibiotic effects. (A) On single-turnover GTPase, final concentrations were ribosomes, 0.5 μM; EF-G, 0.75 μM; and [γ-^{32}P]-GTP, 25 μM. The solid line is fit to Scheme 1 for results obtained in the absence of added antibiotic, as in Figure 5A. (B) On single-turnover P_i release, experiments were carried out as in Figure 6, with a final EF-G concentration of 0.75 μM. (C) On multiple-turnover GTPase, final concentrations were EF-G, 0.5 μM; ribosomes 1.0 μM; and [γ-^{32}P]GTP, 1 mM. For A−C, the insets indicate final antibiotic concentrations after mixing. ThS was preincubated with ribosomes as indicated. FA was either preincubated with ribosomes or with EF-G·GTP as indicated. Concentrations during preincubation were double those shown.

bring G′ closer to L11-NTD when EF-G·GTP is added to the ribosome. These processes differ ~100-fold in apparent rate constant, and only the more rapid one, which involves the larger change in FRET signal, occurs at a rate compatible with the functioning of EF-G during translocation (*34*) or ribosome recycling (*16*). Replacement of GTP by GDPCP results in a biphasic FRET change of similar overall magnitude, signaling the movement of G′ toward L11-NTD, but with apparent rate constants that are ~100-fold and 3000-fold lower than rapid FRET change. These results, which suggest that it is the binding of EF-G·GTP itself that induces changes in the ribosome conformation, with GTP hydrolysis only accelerating the process, are reminiscent of results showing that translocation is much slower when GTP is replaced with nonhydrolyzable GTP analogues (*35*, *39*).

The significance for normal ribosome function of the second, slow FRET change induced by EF-G·GTP is uncertain. L11 is a part of the highly mobile stalk region of the 50S subunit. Particularly pertinent for our experiments is the large displacement recently found for L11 in two crystal forms of the *E. coli* 70S ribosome, in which the positions of the C_αs of Cys 38 are 19 Å apart (*6*). The slow FRET change may arise from EF-G-induced perturbations of this stalk region, which also includes L10, multiple copies of L7/L12, and 23S rRNA nucleotides 1030−1124. Recent structural studies of Diaconu et al. (*40*) have suggested that L11 may function as a bridge between EF-G and the L10-NTD, which anchors the L7/L12 multimer to 23S rRNA. If so, then the G′-L11-NTD distance may be sensitive to conformational changes throughout the stalk region.

The dependence of rapid FRET change on GTP (Figure 3C) qualitatively supports the earlier hypothesis (*10*) that the G′ region of EF-G moves closer to L11-NTD as a result of GTP hydrolysis. However, as a result of slow FRET changes of the kind mentioned above, the G′ region and L11-NTD are considerably closer to one another in static complexes 1 and 2 than in states b and c (Scheme 1) which are found during catalytic turnover of GTP. Thus, the FRET-derived estimates of distance are 89 and 80 Å for states b and c, respectively, whereas the values calculated by extrapolation of the slow FRET changes seen for the GDPCP and FA samples (Figure 3D) to infinite time, which should correspond to those measured for complexes 1 and 2, respectively, are 73 and 67 Å [the fact that these values are slightly larger than those derived from the static experiments in Figure 2 is likely due to small differences in the way that fluorescence was measured in the two kinds of experiments (see the Materials and Methods)].

FA Inhibition. FA acts as a "slow" inhibitor of EF-G·GTPase on the ribosome, decreasing the apparent initial turnover rate and eventually halting GTPase turnover altogether (Figure 8C). This conclusion stands in marked contrast to the prevailing view in the literature, on the basis of an early result of Bodley et al. (*11*), that FA completely inhibits GTPase turnover after one round of GTP hydrolysis, after which it freezes the product EF-G·GDP on the ribosome. However, the Bodley experiment was carried out at an FA concentration of 3 mM, more than *3 orders of magnitude higher* than either the K_i value of 1−2 μM found for FA inhibition of multiple-turnover EF-G·GTPase on the ribosome (*41*, *42*) or the K_d of 0.4 μM for FA binding to the ribosome·EF-G complex in the presence of GDP or GTP (*43*). It is also pertinent to note that, while there is indirect evidence for FA binding to EF-G based on the strong correlation between FA resistance and mutations in EF-G (*44*, *45*), no FA·EF-G·G-nucleotide complex has been demonstrated, so that such a complex, if it exists at all, must be quite weak.

What then is the mode of action of FA? We propose the model shown in Scheme 2. At low concentrations of FA (<50 μM), FA binds exclusively to the ribosome·EF-G·G-nucleotide complex. This binding permits relatively rapid

Scheme 2: Slow Inhibition by Fusidic Acid of EF-G-Dependent GTPase on the Ribosome (R = Ribosome, G = EF-G, and FA = Fusidic Acid)

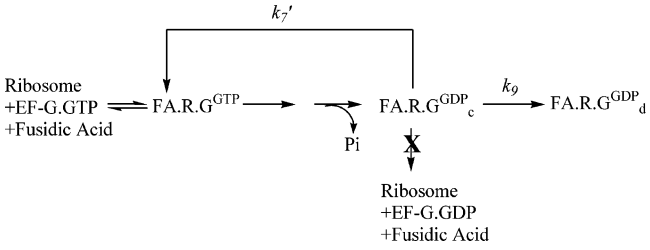

formation of state c, as in Scheme 1, but blocks EF-G release from state c while permitting GDP/GTP exchange via step 7′. The slow phase of FRET change, which is seen in both the absence or presence of FA (Figure 3D), has a much higher amplitude in the presence of FA, corresponding to a closer approach of G′ to L11-NTD. We propose that this closer approach gives rise to a conformation, state d, in which GDP/GTP exchange is blocked, leading to an eventual halt in GTPase turnover. We attribute the decreasing number of GTPase turnovers as the FA concentration is raised well beyond the level needed to saturate the high-affinity site in the ribosome·EF-G·G-nucleotide complex to the formation of a low-affinity, binary FA·EF-G complex prior to ribosome binding. We further speculate that, within this complex, EF-G assumes a conformation that, while permitting GTP hydrolysis on the binding to the ribosome, leads to a rapid formation of state d, thus blocking GDP/GTP exchange. In the limit, full formation of the FA·EF-G·GTP complex prior to ribosome binding, which, from the Bodley et al. (*10*) results, is apparently achieved at an FA concentration ≤3 mM, would lead to the inhibition of GTPase turnover after one round of GTP hydrolysis. Further work will be required to verify this model.

Scheme 1 and Translocation. The most complete kinetic model for EF-G-dependent translocation is that proposed by Savelsbergh et al. (*34*). Despite the important differences between translocating ribosomes and the vacant ribosomes studied here, it is not unreasonable to compare Scheme 1 with the Savelsbergh model, especially because Peske et al. (*46*) have shown that ribosomal antibiotics, which inhibit translocation by inhibiting tRNA−mRNA movement, have no effect on the functional cycle of the EF-G interaction with the ribosome.

Scheme 1 is, in fact, formally identical to the Savelsbergh scheme, in which a ribosomal "unlocking" step that follows GTP hydrolysis limits both P_i release from ribosome-bound EF-G and tRNA−mRNA translocation. Notable quantitative similarities include (a) the equilibrium constant for the initial EF-G·GTP complex formation (this paper, 0.8 ± 0.3 μM, step 1, Savelsbergh et al. (*34*), 0.9 μM) and (b) the values of the rate constants for the unlocking step in Savelsbergh et al. (35 ± 5 s^{-1}) and, for step 3, state a → state b conversion (36 ± 5 s^{-1}). The most significant difference is that the major pathway for P_i release in Scheme 1 proceeds much more slowly (3.6 s^{-1}) than P_i release in translocation (9.4 s^{-1} at 25 °C, *34*), a point that we have recently demonstrated by direct comparison (Pan et al., submitted for publication). This major pathway (steps 4 and 6) differs from the minor pathway (step 5) in that P_i release occurs after rather than before state b → state c conversion, leading to the conclusion that prior G′ to L11-NTD movement retards P_i release. Such movement may be blocked in a translocating ribosome.

In summary, we demonstrate that rapid G′ to L11-NTD movement during single turnover of EF-G·GTPase on the ribosome requires prior GTP hydrolysis and, via branching pathways, either precedes P_i release or occurs essentially simultaneously with it. FA functions as a slow inhibitor of EF-G·GTPase, inducing a closer approach of the G′ region of EF-G to L11-NTD than what is found during normal turnover. This movement inhibits GDP/GTP exchange on ribosome-bound EF-G.

ACKNOWLEDGMENT

This work is supported by NIH Grant GM 071014 (to B. S. C.) and by DFG Grant NI 174/8-1, 2, and 3 (to K. H. N.).

REFERENCES

1. Ban, N., Nissen, P., Hansen, J., Moore, P. B., and Steitz, T. A. (2000) The complete atomic structure of the large ribosomal subunit at 2.4 Å resolution, *Science 289*, 905−920.
2. Harms, J., Schluenzen, F., Zarivach, R., Bashan, A., Gat, S., Agmon, I., Bartels, H., Franceschi, F., and Yonath, A. (2001) High-resolution structure of the large ribosomal subunit from a mesophilic eubacterium, *Cell 107*, 679−688.
3. Schluenzen, F., Tocilj, A., Zarivach, R., Harms, J., Gluehmann, M., Janell, D., Bashan, A., Bartels, H., Agmon, I., Franceschi, F., and Yonath, A. (2000) Structure of functionally activated small ribosomal subunit at 3.3 Å resolution, *Cell 102*, 615−623.
4. Wimberly, B. T., Brodersen, D. E., Clemons, W. M., Jr., Morgan-Warren, R. J., Carter, A. P., Vonrhein, C., Hartsch, T., and Ramakrishnan, V. (2000) Structure of the 30S ribosomal subunit, *Nature 407*, 327−339.
5. Yusupov, M. M., Yusupova, G. Z., Baucom, A., Lieberman, K., Earnest, T. N., Cate, J. H., and Noller, H. F. (2001) Crystal structure of the ribosome at 5.5 Å resolution, *Science 292*, 883−896.
6. Schuwirth, B. S., Borovinskaya, M. A., Hau, C. W., Zhang, W., Vila-Sanjurjo, A., Holton, J. M., and Cate, J. H. (2005) Structures of the bacterial ribosome at 3.5 Å resolution, *Science 310*, 827−834.
7. Thompson, J., Cundliffe, E., and Stark, M. (1979) Binding of thiostrepton to a complex of 23-S rRNA with ribosomal protein L11, *Eur. J. Biochem. 98*, 261−265.
8. Wimberly, B. T., Guymon, R., McCutcheon, J. P., White, S. W., and Ramakrishnan, V. (1999) A detailed view of a ribosomal active site: The structure of the L11−RNA complex, *Cell 97*, 491−502.
9. Agrawal, R. K., Heagle, A. B., Penczek, P., Grassucci, R. A., and Frank, J. (1999) EF-G-dependent GTP hydrolysis induces translocation accompanied by large conformational changes in the 70S ribosome, *Nat. Struct. Biol. 6*, 643−647.
10. Agrawal, R. K., Linde, J., Sengupta, J., Nierhaus, K. H., and Frank, J. (2001) Localization of L11 protein on the ribosome and elucidation of its involvement in EF-G-dependent translocation, *J. Mol. Biol. 311*, 777−787.
11. Bodley, J. W., Zieve, F. J., and Lin, L. (1970) Studies on translocation. 4. The hydrolysis of a single round of guanosine triphosphate in the presence of fusidic acid, *J. Biol. Chem. 245*, 5662−5667.
12. Frank, J., and Agrawal, R. K. (2000) A ratchet-like inter-subunit reorganization of the ribosome during translocation, *Nature 406*, 318−322.
13. Rodnina, M. V., Savelsbergh, A., Matassova, N. B., Katunin, V. I., Semenkov, Y. P., and Wintermeyer, W. (1999) Thiostrepton inhibits the turnover but not the GTPase of elongation factor G on the ribosome, *Proc. Natl. Acad. Sci. U.S.A. 96*, 9586−9590.
14. Cameron, D. M., Thompson, J., March, P. E., and Dahlberg, A. E. (2002) Initiation factor IF2, thiostrepton and micrococcin prevent the binding of elongation factor G to the *Escherichia coli* ribosome, *J. Mol. Biol. 319*, 27−35.
15. Cameron, D. M., Thompson, J., Gregory, S. T., March, P. E., and Dahlberg, A. E. (2004) Thiostrepton-resistant mutants of *Thermus thermophilus*, *Nucleic Acids Res. 32*, 3220−3227.

16. Seo, H. S., Kiel, M., Pan, D., Raj, V. S., Kaji, A., and Cooperman, B. S. (2004) Kinetics and thermodynamics of RRF, EF-G, and thiostrepton interaction on the *Escherichia coli* ribosome, *Biochemistry 43*, 12728−12740.
17. Hausner, T. P., Atmadja, J., and Nierhaus, K. H. (1987) Evidence that the G2661 region of 23S rRNA is located at the ribosomal binding sites of both elongation factors, *Biochimie 69*, 911−923.
18. Hausner, T. P., Geigenmuller, U., and Nierhaus, K. H. (1988) The allosteric three-site model for the ribosomal elongation cycle. New insights into the inhibition mechanisms of aminoglycosides, thiostrepton, and viomycin, *J. Biol. Chem. 263*, 13103−13111.
19. Cooperman, B. S., Vladimirov, S., Bukhtiyarov, Y., Druzina, Z., Wang, R., and Seo, H. S. (2000), Applying photolabile derivatives of oligonucleotides to probe the peptidyl transferase center, in *Ribosome: Structure, Function, Antibiotics, and Cellular Interactions* (Garrett, R. Ed.) pp 271−285, American Society for Microbiology, Washington, DC.
20. Druzina, Z., and Cooperman, B. S. (2004) Photolabile anticodon stem-loop analogs of tRNAPhe as probes of ribosomal structure and structural fluctuation at the decoding center, *RNA 10*, 1550−1562.
21. Wang, R., Alexander, R. W., VanLoock, M., Vladimirov, S., Bukhtiyarov, Y., Harvey, S. C., and Cooperman, B. S. (1999) Three-dimensional placement of the conserved 530 loop of 16 S rRNA and of its neighboring components in the 30 S subunit, *J. Mol. Biol. 286*, 521−540.
22. Stoffler, G., Cundliffe, E., Stoffler-Meilicke, M., and Dabbs, E. R. (1980) Mutants of *Escherichia coli* lacking ribosomal protein L11, *J. Biol. Chem. 255*, 10517−10522.
23. Brune, M., Hunter, J. L., Corrie, J. E., and Webb, M. R. (1994) Direct, real-time measurement of rapid inorganic phosphate release using a novel fluorescent probe and its application to actomyosin subfragment 1 ATPase, *Biochemistry 33*, 8262−8271.
24. Rosendahl, G., and Douthwaite, S. (1993) Ribosomal proteins L11 and L10·(L12)4 and the antibiotic thiostrepton interact with overlapping regions of the 23 S rRNA backbone in the ribosomal GTPase centre, *J. Mol. Biol. 234*, 1013−1020.
25. Wendrich, T. M., Blaha, G., Wilson, D. N., Marahiel, M. A., and Nierhaus, K. H. (2002) Dissection of the mechanism for the stringent factor RelA, *Mol. Cell 10*, 779−788.
26. Wahler, B. E., and Wollenberger, A. (1958) Determination of orthophosphate in the presence of phosphate compounds with an affinity for acids and molybdate, *Biochem. Z. 329*, 508−520.
27. Lakowicz, J. R. (1999) *Principles of Fluorescence Spectroscopy*, 2nd ed., Kluwer Academic/Plenum Press, New York.
28. Harris, D. C. (1995) *Quantitative Chemical Analysis*, 4th ed., W. H. Freeman and Company, New York.
29. Reynolds, G. A., and Drexhage, K. H. (1975) New coumarin dyes with rigidized structure for flashlamp-pumped dye lasers, *Opt. Commun. 13*, 222−225.
30. Conrad, R. H., and Brand, L. (1968) Intramolecular transfer of excitation from tryptophan to 1-dimethylaminonaphthalene-5-sulfonamide in a series of model compounds, *Biochemistry 7*, 777−787.
31. Odom, O. W., Deng, H. Y., Dabbs, E. R., and Hardesty, B. (1984) Binding of S21 to the 50S subunit and the effect of the 50S subunit on nonradiative energy transfer between the 3′ end of 16S RNA and S21, *Biochemistry 23*, 5069−5076.
32. Thielen, T. P. G. M., Maassen, J. A., Kriek, J., and Moller, W. (1984) Dimer structure of the ribosomal protein L7/L12 probed by energy transfer, *Biochemistry 23*, 6668−6674.
33. Agrawal, R. K., Penczek, P., Grassucci, R. A., and Frank, J. (1998) Visualization of elongation factor G on the *Escherichia coli* 70S ribosome: The mechanism of translocation, *Proc. Natl. Acad. Sci. U.S.A. 95*, 6134−6138.
34. Savelsbergh, A., Katunin, V. I., Mohr, D., Peske, F., Rodnina, M. V., and Wintermeyer, W. (2003) An elongation factor G-induced ribosome rearrangement precedes tRNA−mRNA translocation, *Mol. Cell 11*, 1517−1523.
35. Zavialov, A. V., Hauryliuk, V. V., and Ehrenberg, M. (2005) Guanine-nucleotide exchange on ribosome-bound elongation factor G initiates the translocation of tRNAs, *J. Biol. 4*, 9.
36. Cleland, W. W. (1975) Partititon analysis and the concept of net rate constants as tools in enzyme kinetics, *Biochemistry 14*, 3220−3224.
37. dos Remedios, C. G., and Moens, P. D. (1995) Fluorescence resonance energy transfer spectroscopy is a reliable "ruler" for measuring structural changes in proteins. Dispelling the problem of the unknown orientation factor, *J. Struct. Biol. 115*, 175−185.
38. Parkhurst, L. J., Parkhurst, K. M., Powell, R., Wu, J., and Williams, S. (2001) Time-resolved fluorescence resonance energy transfer studies of DNA bending in double-stranded oligonucleotides and in DNA−protein complexes, *Biopolymers 61*, 180−200.
39. Katunin, V. I., Savelsbergh, A., Rodnina, M. V., and Wintermeyer, W. (2002) Coupling of GTP hydrolysis by elongation factor G to translocation and factor recycling on the ribosome, *Biochemistry 41*, 12806−12812.
40. Diaconu, M., Kothe, U., Schlunzen, F., Fischer, N., Harms, J. M., Tonevitsky, A. G., Stark, H., Rodnina, M. V., and Wahl, M. C. (2005) Structural basis for the function of the ribosomal L7/12 stalk in factor binding and GTPase activation, *Cell 121*, 991−1004.
41. Okura, A., Kinoshita, T., and Tanaka, N. (1971) Formation of fusidic acid−G factor−GDP−ribosome complex and the relationship to the inhibition of GTP hydrolysis, *J. Antibiot. 24*, 655−661.
42. Burdett, V. (1996) Tet(M)-promoted release of tetracycline from ribosomes is GTP dependent, *J. Bacteriol. 178*, 3246−3251.
43. Willie, G. R., Richman, N., Godtfredsen, W. P., and Bodley, J. W. (1975) Some characteristics of and structural requirements for the interaction of 24,25-dihydrofusidic acid with ribosome−elongation factor G complexes, *Biochemistry 14*, 1713−1718.
44. Johanson, U., and Hughes, D. (1994) Fusidic acid-resistant mutants define three regions in elongation factor G of *Salmonella typhimurium*, *Gene 143*, 55−59.
45. Laurberg, M., Kristensen, O., Martemyanov, K., Gudkov, A. T., Nagaev, I., Hughes, D., and Liljas, A. (2000) Structure of a mutant EF-G reveals domain III and possibly the fusidic acid binding site, *J. Mol. Biol. 303*, 593−603.
46. Peske, F., Savelsbergh, A., Katunin, V. I., Rodnina, M. V., and Wintermeyer, W. (2004) Conformational changes of the small ribosomal subunit during elongation factor G-dependent tRNA−mRNA translocation, *J. Mol. Biol. 343*, 1183−1194.

BI0516677